Origin of Lapse Rate Changes in the Upper Tropical Troposphere

IAN FOLKINS

Atmospheric Science Program, Department of Oceanography, Dalhousie University, Halifax, Nova Scotia, Canada

(Manuscript received 6 November 2000, in final form 21 August 2001)

ABSTRACT

Vertical motions in clouds arise from a variety of thermodynamic processes, including latent heat release, evaporative cooling, melting, and cloud radiative heating. In the Tropics, the net upward vertical mass flux from convective systems should approximately balance subsidence in clear sky regions associated with radiative cooling, provided the exchange of mass with midlatitudes can be assumed small. Tropical climatologies of temperature, water vapor, and ozone are used to calculate the clear sky radiative mass flux, and the derivative of this mass flux with respect to potential temperature, $dM_r(\theta)/d\theta$, is used as a proxy for net convective outflow. Convective outflow increases rapidly at 345 K (~11.3 km). This corresponds to the pseudoequivalent potential temperature θ_e at which air parcels near the surface first attain positive convective available potential energy (CAPE). The rate at which $dM_r(\theta)/d\theta$ decreases above 345 K is similar to the rate at which the near surface θ_e probability distribution function (PDF) decreases. This behavior is referred to as ''scaling.'' It suggests that the timescale for removal of an air parcel from the convective boundary layer is independent of θ_e (once it has positive CAPE), and that the residual vertical mass flux from convective clouds can be described as if air parcels detrain near their level of neutral buoyancy (LNB). It is also suggested that the mean tropical temperature profile above 345 K is controlled, not by mixing, but by the need for the vertical variation in net convective outflow to be consistent with the near-surface θ_e PDF, and that this accounts for the fact that the mean temperature profile above 345 K increasingly deviates from a moist adiabat. It is also argued that there are sufficient high θ_e air parcels near the surface to sustain the Brewer–Dobson circulation by detrainment at the LNB followed by radiative ascent into the stratosphere.

1. Introduction

It has long been anticipated that there should be some relationship between the distribution of temperature and humidity near the surface in the Tropics and the variation of convective outflow with height in the upper troposphere (e.g., Reid and Gage 1981; Chimonas and Rossi 1987; Selkirk 1993). This is based on the notion that an air parcel rising from the surface should detrain near its level of neutral buoyancy (LNB). This is true only if no mixing occurs during the ascent. Air parcels that mix with cooler and dryer air during their ascent can be expected to detrain below the LNB, whereas air parcels that overshoot the LNB and mix with warmer ambient air can be expected to detrain above the LNB. In an earlier paper, it was shown that despite this limitation, the LNB concept could be used to motivate a simple relationship between the statistical distribution of pseudoequivalent potential temperature (θ_e) near the surface and the downward clear sky mass flux in the the upper tropical troposphere (Folkins et al. 2000). This paper will discuss this relationship in greater detail, and why this relationship helps constrain the large-scale temperature structure of the upper tropical troposphere.

2. The statistical distribution of θ_e near the surface

Figure 1 shows two ways of representing the statistical distribution of pseudoequivalent potential temperature below 850 mb in the Tropics. Figure 1b shows the cumulative distribution function (CDF) obtained by counting the number of air parcels whose θ_e is larger than a given value, and then normalizing this number by total number of measurements. This distribution will be referred to as $N(\theta_e)$. Figure 1a shows the probability distribution function (PDF) obtained by counting the number of measurements within 1-K θ_e bins, and then normalizing the distribution so that the integrated probability from 310 to 380 K is equal to one. This distribution will be referred to as $-dN(\theta_e)/d\theta_e$. It is nearly symmetric about a peak value at 345 K.

The pseudoequivalent potential temperatures used to infer the distributions shown in Fig. 1 were calculated (Bolton 1980) using temperature and humidity measurements from the Forecast Systems Laboratory National Climatic Data Center (FSL NCDC) Radiosonde Archive. The tropical radiosonde locations used by this

Corresponding author address: Dr. Ian Folkins, Department of Oceanography, Dalhousie University, Halifax, NS B3H 4J1, Canada. E-mail: Ian.Folkins@dal.ca

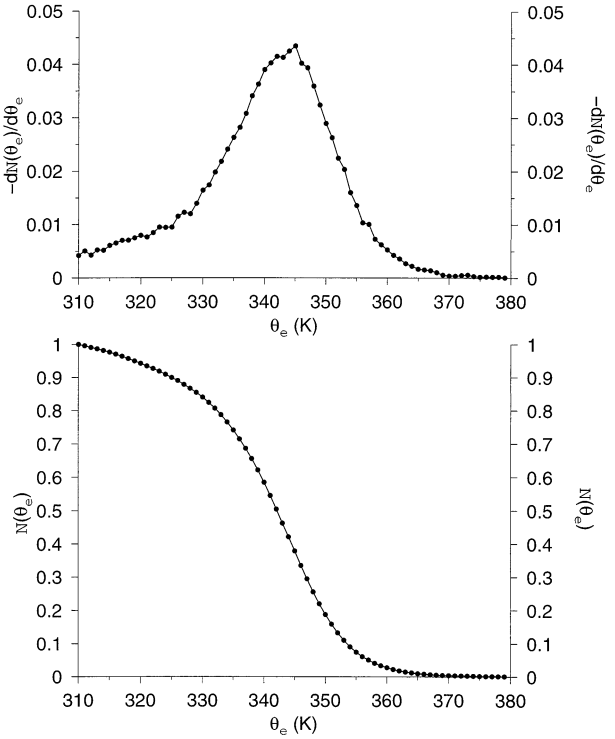

FIG. 1. (a) The PDF of tropical (15°S–15°N), near-surface (below 850 mb) pseudoequivalent potential temperatures. The distribution has been normalized so that the integrated probability from 310 to 380 K is equal to one. The decrease in the PDF above 345 K is probably associated with the preferential removal of positive CAPE air parcels by deep convection. (b) The CDF corresponding to the PDF given in (a).

archive are shown in Fig. 2. Since we wanted to focus on regions where deep convection was likely to occur, only those radiosondes launched between 15°S and 15°N were used. We used one complete year of data from January to December of 1999. In principle, the distributions can be calculated by simply counting the number of θ_e measurements below 850 mb. However many of the radiosonde measurements occur at the standard pressure levels of 1000, 925, 850 mb, etc. To ensure that each pressure interval contributed equally, we first calculated a $N(\theta_e)$ and $-dN(\theta_e)/d\theta_e$ for each 10-mb layer between 1000 and 850 mb using only measurements from within that pressure interval. The distributions from the various pressure intervals were than averaged to produce the curves shown in Fig. 1.

It will be argued later that air parcels become able to participate in deep convection once their θ_e becomes larger than 345 K. This suggests that the variation of net convective outflow with height in the upper tropical troposphere should be determined in part by the shape of the θ_e distributions for $\theta_e > 345$ K. Figure 3 shows the CDFs obtained by counting θ_e measurements between the 1000-mb level and the six top pressure levels of 950, 900, 850, 800, 750, and 700 mb. Each of the CDFs has been in this case normalized to 1 at 345 K.

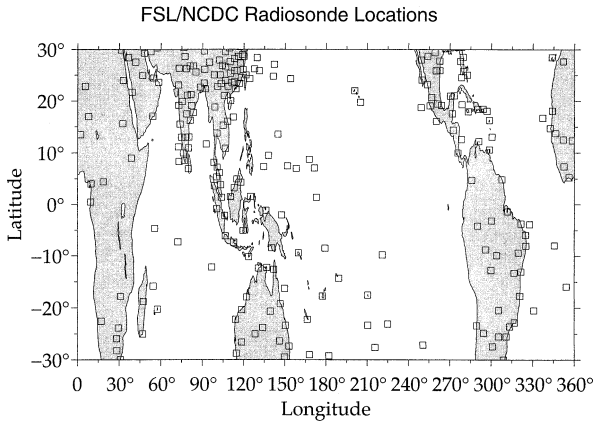

FIG. 2. The radiosonde locations used in the FSL NCDC data archive.

Here $N(\theta_e)$ is somewhat larger for the largest pressure cutoffs, since the higher θ_e air parcels tend to be located closer to the surface. As however the pressure cutoff is reduced, the shape of the CDFs converges to a common, approximately exponential, functional form. In particular, the $N(\theta_e)$ calculated using pressure cutoffs of 800, 750, and 700 mb are virtually identical. This is because air parcels with θ_e larger than 345 K are very rare above 800 mb. This is shown in Fig. 4. The fraction of air parcels with θ_e larger than 345 K is plotted as a function of pressure for the years 1999 and 2000. In both years, fewer than 5% of the air parcels above 800 mb have θ_e larger than 345 K. Near the surface, the fraction of air parcels with $\theta_e > 345$ K is somewhat larger in 2000 than 1999.

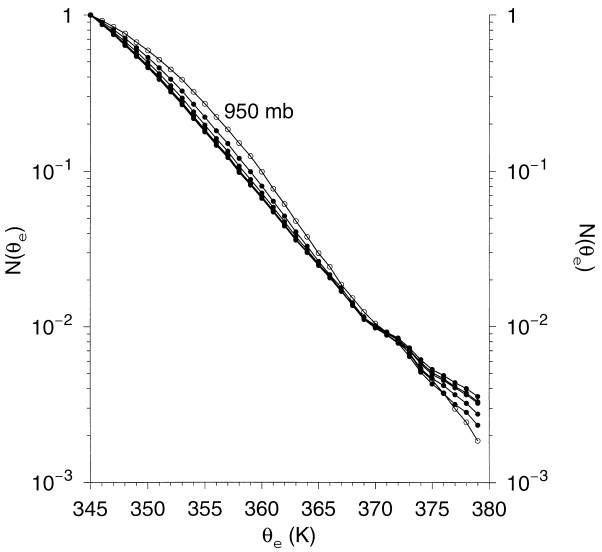

FIG. 3. Each curve represents a CDF obtained using a different pressure cutoff. The CDF drawn in open circles was obtained with a pressure cutoff of 950 mb. The curves below were obtained using cutoffs of 900, 850, 800, 750, and 700 mb. Each curve has been normalized to 1 at 345 K, to emphasize that differences in shape between the 800-, 750-, and 700-mb curves are small.

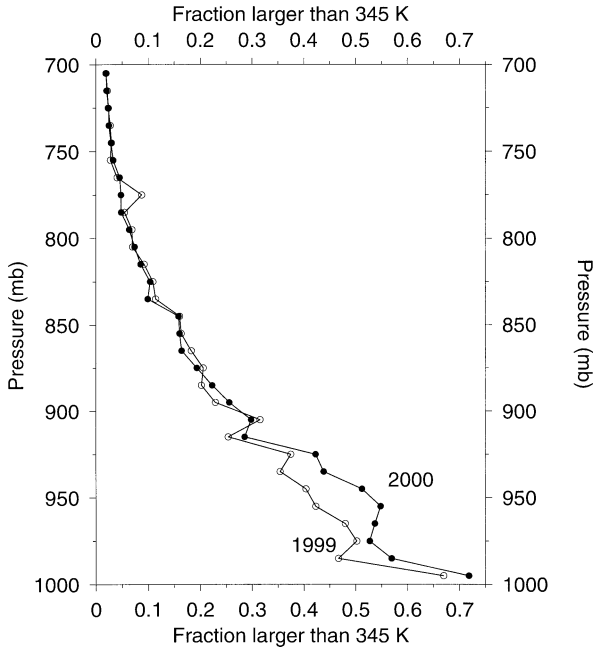

FIG. 4. The fraction of air parcels with $\theta_e > 345$ K, within each 10-mb interval from 1000 to 700 mb. The curve drawn in open circles was obtained from FSL NCDC data from 1999, while the curve in solid circles was obtained from 2000 data.

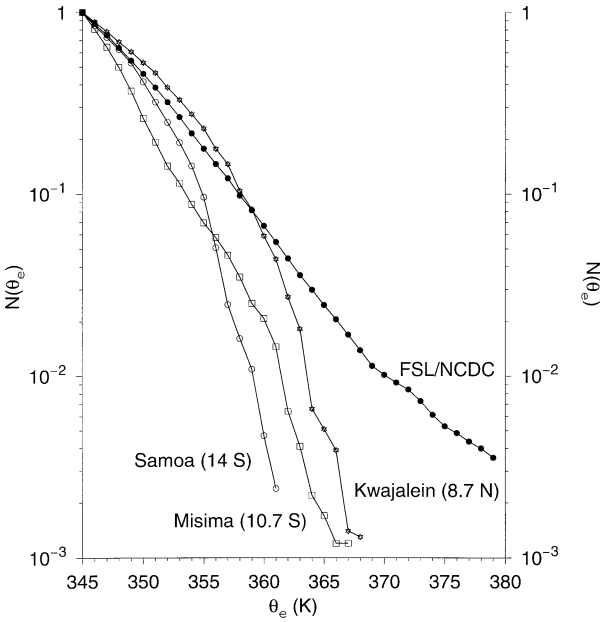

FIG. 5. Each curve represents a CDF (normalized to 1 at 345 K) from a different dataset. The FSL NCDC CDF is larger than the others for $\theta_e > 365$ K.

The fact that air parcels with $\theta_e > 345$ K are rarely found above 800 mb is probably because the upward transport of heat and moisture from the surface by boundary layer clouds over the tropical oceans is typically capped at 800 mb, which is considered to be the mean top of convective boundary layer (CBL) (e.g., Betts and Ridgway 1989).

There are significant regional variations in the θ_e distribution functions. Figure 5 shows various CDFs, all normalized so that N (345 K) = 1, and all obtained from radiosonde measurements below 700 mb. The CDF from Samoa (14°S) was calculated from 175 sondes launched between 1995 and 1999 as part of Pacific Exploratory Mission Tropics A and B campaigns, while the CDFs from Kwajalein (8.7°N) and Misima (10.7°S) were calculated from sondes launched between November 1992 and February 1993 of the TOGA–COARE campaign (Tropical Oceans Global Atmosphere Coupled Ocean–Atmosphere Response Experiment). Both of these locations are within the western Pacific warm pool. The CDF at Kwajalein is characteristic of the highest θ_e PDFs from TOGA COARE. There appears to be significant monthly variability at each site, perhaps partly responding to changes in the intensity of convection, which tends to decrease the CDFs by preferentially removing air parcels with $\theta_e > 345$ K. The FSL NCDC CDF is broadly representative of the CDFs observed from TOGA COARE, perhaps reflective of the fact that many of the FSL NCDC locations between 15°S and 15°N occur in the western Pacific, and the fact that the higher θ_e regions naturally dominate the shape of the CDFs for $\theta_e > 345$ K. The FSL NCDC CDF does however differ significantly from the others in that it has a much larger $N(\theta_e)$ for $\theta_e > 365$ K.

The difference between θ_e and θ is typically largest at the surface and tends to decrease with height as the water vapor concentration diminishes. Figure 6 shows

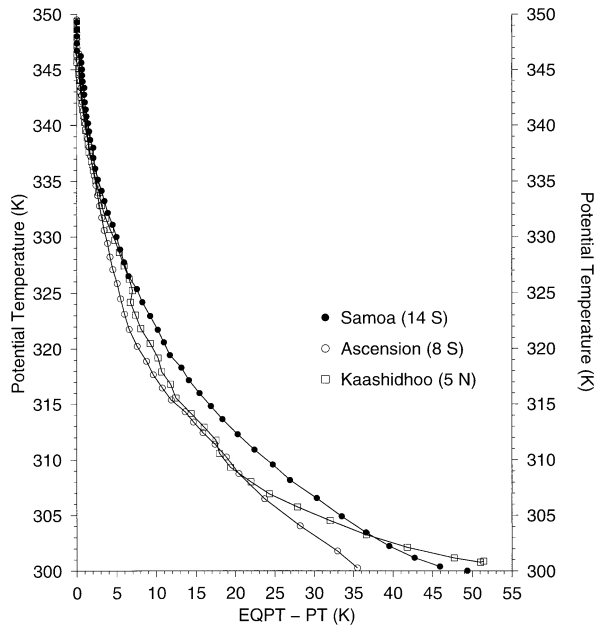

FIG. 6. A vertical profile of $\theta_e - \theta$ [labeled EQPT-PT(K)] obtained from annual climatologies of pressure, temperature, and relative humidity at three different tropical locations. At all three locations, the difference goes to zero near 345 K.

the dependence of $\theta_e - \theta$ on potential temperature at three tropical locations. We have used the mean temperature and humidity profiles of Samoa (14°S), Ascension (8°S), and Kaashidhoo (5°N). Sondes at these last two locations were obtained from the SHADOZ dataset [Southern Hemisphere Additional Ozonesondes project (Thompson et al. 2001, manuscript submitted to *J. Geophys. Res.*)]. Above 345 K (~11.3 km), the difference between θ_e and θ is very small (all conversions between height and potential temperature in this paper are from annual 15°S–15°N climatologies). Although this difference will be slightly larger for an air parcel that is detraining from a convective cloud and has near 100% relative humidity, it indicates that an air parcel undergoing undilute, pseudoadiabatic ascent within a cloud will detrain very near the height at which its θ_e becomes equal to the θ of the background atmosphere.

In pseudoadiabatic ascent, any water that condenses in the air parcel is assumed to be immediately removed. This ignores possible additional heat releases associated with the conversion of water to ice, which can increase the final θ of the air parcel by several Kelvins or more. In addition, removal of condensate after a delay tends to increase the final θ_e since the condensate leaves the air parcel at a lower temperature than it would otherwise. These additional θ_e increases may be partially mitigated by an increase in the specific heat of the air parcel associated with the retention of the condensate (Williams and Renno 1993).

3. Clear sky radiative mass fluxes

In the Tropics, convective systems are typically associated with complex patterns of upward and downward motions driven by latent heat release, evaporative cooling, ice melting, turbulent mixing, cloud radiative effects, and gravity waves (Gamache and Houze 1982; Johnson 1982). In this paper, the residual divergence arising from these vertical motions will be referred to as ''net convective outflow,'' with the understanding that this term does not refer simply to the outflows associated with convective detrainment.

Averaged over the Hadley cell, the net upward transport of mass within convective systems will be balanced by the downward mass flux in clear sky regions associated with radiative cooling (provided the exchange of mass and energy between the Tropics and midlatitudes can be ignored). The subsidence associated with clear sky radiative cooling is given by

$$M_r(\theta) = \rho(\theta) w_r(\theta) = \rho(\theta) Q_r(\theta)/[dT(\theta)/dz + \Gamma_d], \quad (1)$$

where $dT(\theta)/dz$ is the derivative of temperature with respect to height, Γ_d is the dry-adiabatic lapse rate, $\rho(\theta)$ is density, $w_r(\theta)$ the downward radiative velocity, and $Q_r(\theta)$ the clear sky radiative cooling rate. This expression is valid in clear sky regions over long timescales where the heights of potential temperature surfaces can be regarded as fixed.

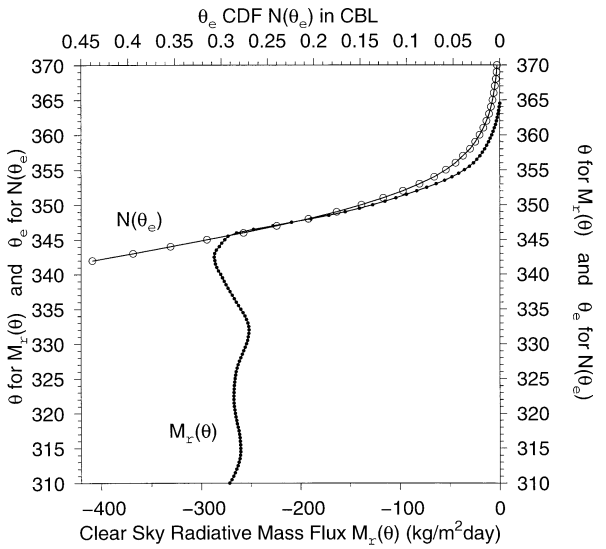

FIG. 7. The plot with solid circles is the clear sky radiative mass flux $M_r(\theta)$. The mass flux was evaluated from the $\pm 30°$ temperature and heating rates using (1) in the text. The plot with open circles shows the variation of $N(\theta_e)$ with pseudoequivalent potential temperature (using the 800-mb pressure cutoff). The horizontal axis of $M_r(\theta)$ has been scaled to emphasize that $M_r(\theta)$ and $N(\theta_e)$ decrease in a similar manner for $\theta > 345$ K.

Figure 7 shows the variation of the clear sky radiative mass flux $M_r(\theta)$ calculated using (1). The clear sky heating rate used in (1) was calculated using a radiative transfer model based on the δ-four-stream method (Fu and Liou 1992). This model requires vertical profiles of temperature, water vapor mixing ratio, ozone, and pressure versus height. It was run from 0 to 50 km at 0.25-km resolution. The diurnal average was obtained using a 1-h time step. The subsidence term $M_r(\theta)$ was first calculated for every month and for every 5° latitude bin from 30°S to 30°N and then averaged over these profiles using an appropriate areal weighting to produce the 1999 30°S–30°N average shown in Fig. 7. When adding mass fluxes defined over different latitude ranges, each mass flux was first interpolated to a common potential temperature grid. Monthly temperature climatologies within each latitude bin were obtained from the FSL NCDC radiosonde archive using the standard pressure level measurements at 1000, 925, 850, 700, 500, 400, 300, 250, 200, 150, 100, 70, 50, 30, 20, and 10 mb. Spline interpolation in height was used to obtain temperatures on the model grid below 10 mb. Above 30 km (or sometimes lower where there was insufficient radiosonde data), we used a tropical temperature climatology from the Air Force Geophysics Laboratory (Anderson et al. 1986). Below 8 km, relative humidities were constrained by the radiosonde measurements. At 12.5 km, a seasonally varying relative humidity climatology obtained from the Microwave Limb Sounder (MLS) was used (Read et al. 2001, hereafter RW01).

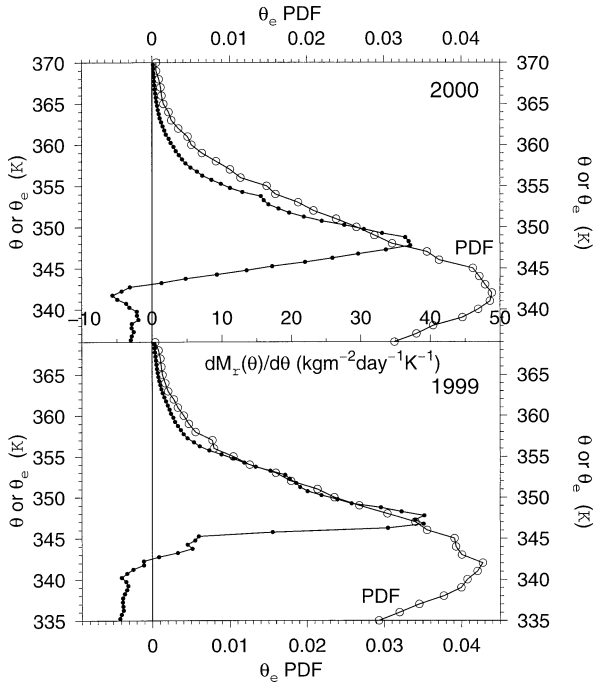

FIG. 8. In both panels, the curve with solid circles is $dM_r(\theta)/d\theta$, the component of the convective outflow balanced by radiative heating. The curve with open circles is the θ_e PDF $dN(\theta_e)/d\theta_e$: (top) 2000 and (bottom) 1999.

Above 18 km a seasonally varying water vapor mixing ratio was imposed, with a minimum of 2.5 ppmv in January and a maximum of 5.0 ppmv in July, close to an annual mean of 3.8 ppmv (Dessler 1998). Spline interpolation in height was again used to define the relative humidities in the model between 8 and 12.5 km, and between 12.5 and 18 km. Below 100 mb, a monthly and latitudinally resolved tropospheric ozone climatology (Logan et al. 1999) was used, while a standard tropical ozone climatology (Anderson et al. 1986) was used above 100 mb.

Figure 7 shows that while $M_r(\theta)$ is fairly constant below 345 K (~11.3 km), $M_r(\theta)$ rapidly decreases above 345 K. The rate of decrease is roughly proportional to $N(\theta_e)$, with in this case the vertical axis referring to θ_e rather than θ.

Figure 8 shows that the decrease in $M_r(\theta)$ above 345 K is associated with a rapid increase in ''net convective outflow,'' as inferred from the variation of $dM_r(\theta)/d\theta$ with θ. In both 1999 and 2000, the rate of decrease in net convective outflow is similar to the decrease in the PDF for that year (shown using open circles). This suggests that the net convective outflow between two nearby θ surfaces in the upper tropical troposphere is roughly proportional to the frequency with which the corresponding value of θ_e is realized in the CBL. This is what one would anticipate under the following conditions: that air parcels become able to participate in deep convection once their θ_e becomes larger than 345 K, every air parcel in the CBL with $\theta > 345$ K is equally subject to deep convection (i.e., the removal timescale is independent of θ_e), air parcels detrain near their LNB, and mass exchange with midlatitudes can be ignored. Although these conditions are unlikely to be satisfied during individual convective events, they may be approximately satisfied when averaged over the Hadley cell, and over sufficiently long timescales.

If in addition we also suppose that all of the downward clear sky mass flux through a potential temperature surface above 345 K (~11.3 km) arises from deep convective outflow at a higher potential temperature, then the mass flux $M_r(\theta)$ should be proportional to $N(\theta_e)$. Figure 7 suggests that this is also approximately correct. It would hold under the additional restriction that the net convective outflow above a θ surface is much larger than the component of that outflow that subsequently ascends into the stratosphere (or is exchanged with midlatitudes at upper tropical tropospheric levels).

The ratio of $dN(\theta_e)/d\theta_e$ to $dM_r(\theta)/d\theta$ can be expressed as a timescale. Let ΔP represent the pressure difference (in mb) between the top and bottom of the surface layer over which a PDF is defined. Let g be the gravitational acceleration. Then $[dN(\theta_e)/d\theta_e](\Delta P/g)$ represents the mass of air parcels per unit area per degree K near the surface whose pseudoequivalent potential temperature is θ_e. The deep convective outflow at the corresponding θ surface can be regarded as the rate of removal, so dividing by $dM_r(\theta)/d\theta$ gives a timescale, τ_{rem}, that can be physically interpreted as the timescale over which deep convection removes ''convective'' air parcels from the boundary layer:

$$\tau_{\text{rem}}(\theta_e) = \frac{dN(\theta_e)/d\theta_e}{dM_r(\theta)/d\theta}\frac{\Delta P}{g}. \tag{2}$$

This timescale has been plotted versus θ in Fig. 9. We have used a 1000–800-mb CBL surface layer (ΔP = 200 mb). The various curves have been generated using $dM_r(\theta)/d\theta$ defined over latitudinal ranges of $\pm 5°$, $\pm 10°$, $\pm 15°$, $\pm 20°$, $\pm 25°$, and $\pm 30°$. In the interval between 345 K (~11.3 km) and 356 K (~15.0 km), where τ_{rem} is reasonably constant for all latitude ranges, the smallest τ_{rem} are those for which the convective outflow is more narrowly defined about the equator, since this is where $dM_r(\theta)/d\theta$ is maximized. The $\pm 30°$ τ_{rem} has been drawn using open circles. In 1999 and 2000, the $\pm 30°$ τ_{rem} is approximately equal to 2 days from 345 to 356 K, increasing to 3 to 5 days between 356 and 370 K. This degree of variation is remarkably small, given that $dM_r(\theta)/d\theta$ varies by a factor of about 200 between 345 and 370 K.

The near constancy of τ_{rem} between 345 and 356 K (and perhaps up to 365 K) is referred to as ''scaling.'' The $\pm 30°$ τ_{rem} is most nearly constant over the broadest range of θ values. This is perhaps not surprising. While $dN(\theta_e)/d\theta_e$ should be defined over the latitudinal range where most deep convection occurs, $dM_r(\theta)/d\theta$ should

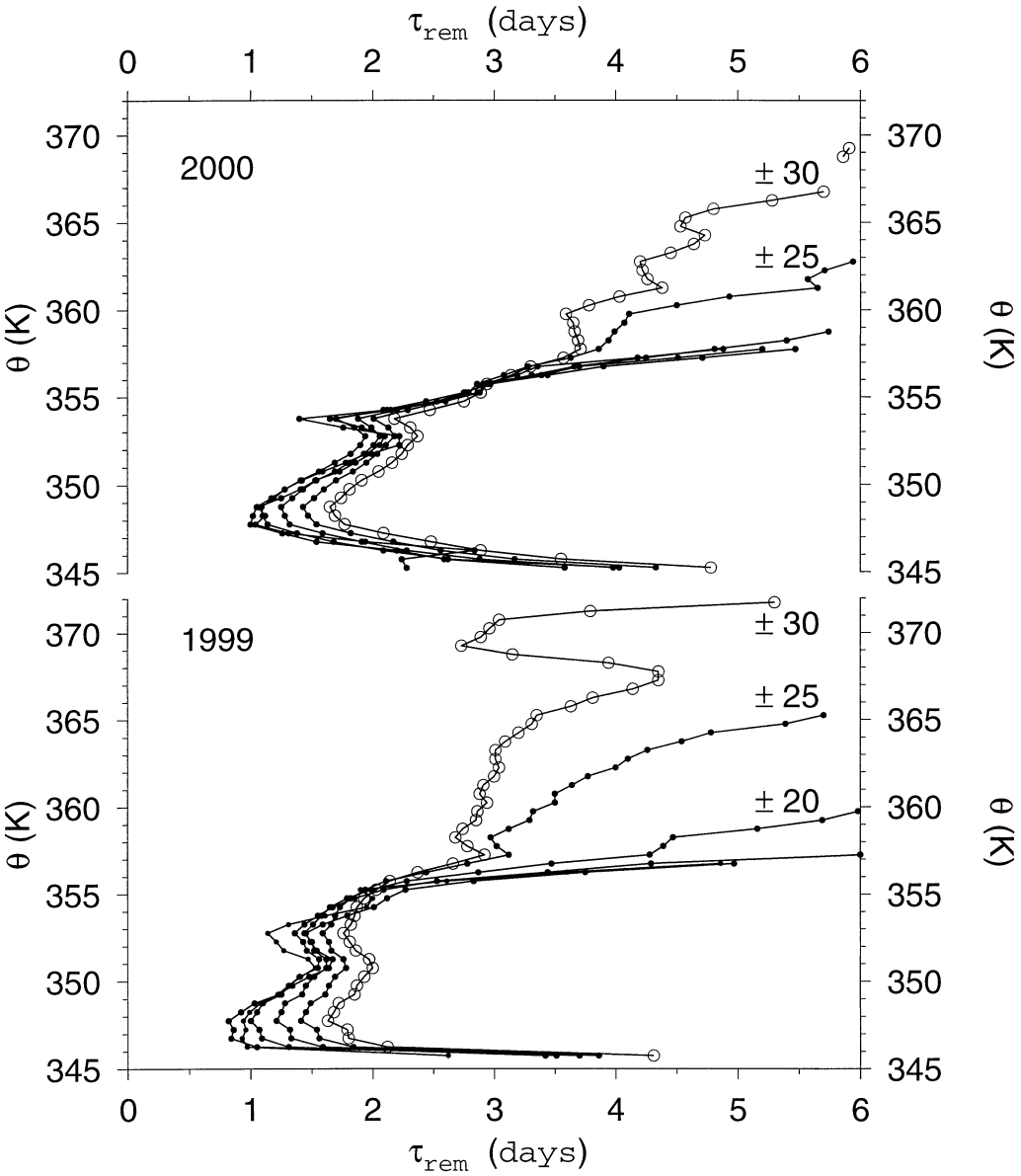

FIG. 9. Each curve refers to τ_{rem} as defined in (2), calculated using $dM_r(\theta)/d\theta$ defined over different latitude ranges. The curve with open circles refers to a latitude range of $\pm 30°$. Generally the curves with the smallest τ_{rem} between 345 and 356 K refer to the latitude ranges closest to the equator: (top) 2000 and (bottom) 1999.

be defined over the latitudinal range where the subsidence associated with this deep convection takes place. An average from 30°S to 30°N is perhaps most appropriate because it encompasses the two subsiding branches of the Hadley cell.

An element of ambiguity enters into the physical interpretation of τ_{rem} as defined in (2), because while $dN(\theta_e)/d\theta_e$ is defined from 15°S to 15°N, $dM_r(\theta)/d\theta$ is defined over a variety of latitude intervals. In particular, if one uses the $dM_r(\theta)/d\theta$ defined from 30°S to 30°N, and if the contribution of convection outside 15°S–15°N is assumed small, τ_{rem} overestimates the real removal time of convective air parcels from the boundary layer by almost a factor of two. Figure 9 therefore suggests that the real removal time of convective air parcels from the boundary layer by deep convection is probably around 1.5 days, at least between 345 and 356 K. Consideration of shallow convection would decrease this number still further.

It is conceivable that the increase in the $\pm 30°$ τ_{rem} toward larger values of θ_e shown in Fig. 9 occurs because extremely high values of θ_e are more likely to occur where convection is suppressed (but sea surface temperatures are still high). However the statistical representativeness of our PDFs becomes more uncertain at higher values of θ_e (see Fig. 5). It is also possible, as

will be discussed later, that the increase in τ_{rem} above 356 K reflects an increasing degree of control on the temperature profile by the Brewer–Dobson circulation.

Also note that although mass flux scaling has been motivated with a very simple picture of tropical convection, the existence of scaling does not imply that this simple picture is realistic. For example, overshooting deep convection, which is accompanied by irreversible mixing of cooler overshooting air with warmer air above the LNB, does inject mass above the LNB. However the new mixed air parcel will have a smaller potential temperature than the previous unmixed air parcel, so that subsidence must eventually accompany the irreversible mixing (Sherwood and Dessler 2001). If these upward and downward mass fluxes cancel, overshooting and irreversible mixing are not inconsistent with the existence of mass flux scaling. A similar argument would apply to detrainment below the LNB.

4. Convective available potential energy

Convective available potential energy (CAPE) is often used as a diagnostic to indicate whether an air parcel is able to participate in deep convection. It is defined as the work done on an air parcel by the atmosphere as the parcel is raised from its level of free convection (LFC) to its (LNB).

$$\text{CAPE} = \int_{\text{LFC}}^{\text{LNB}} (T_{vp} - T_{vb}) R_d \, d \ln P. \qquad (3)$$

The LFC is defined as the height at which the buoyancy force on an air parcel first becomes directed upward. Here T_{vp} and T_{vb} are the virtual temperatures of the parcel and background atmosphere. The gas constant of dry air is R_d and P represents pressure. Figure 10 shows how CAPE typically depends on near-surface θ_e. The pseudoequivalent potential temperature was varied by increasing the temperature while keeping a fixed relative humidity of 0.75. Since the contribution of differences in water vapor concentration to density differences between the air parcel and the ambient atmosphere are usually small, we approximated T_{vp} and T_{vb} by their actual temperatures. The temperature of the air parcel was calculated by assuming conservation of potential temperature below the condensation level and conservation of pseudoequivalent potential temperature above. The ambient temperature profile was a 1999 FSL NCDC average from 15°S to 15°N.

In Fig. 10, the curve with open circles was calculated using CAPE as defined in (3). The curve with solid circles shows the change in CAPE when it is integrated from the surface rather than from the LFC. Both curves indicate that it becomes thermodynamically possible for air parcels near the surface to participate in deep convection once their θ_e becomes larger than 345 K. This threshold should be nearly independent of location between 15°S and 15°N since temperatures within this latitude interval are quite uniform. At a relative humidity of 0.75, θ_e = 345 K corresponds to a surface temperature of 299.54 K (26.4°C). The mean surface temperature between 15°S and 15°N in the FSL NCDC dataset is 299.3 K (26.15°C), while the mean surface RH_{water} water is 0.79 (θ_e = 346.5 K). The proximity of these values of θ_e is unsurprising. The tropical atmosphere is approximately moist adiabatic below 11 km. One would therefore expect an air parcel at the surface with a temperature equal to the surface mean to have near zero CAPE.

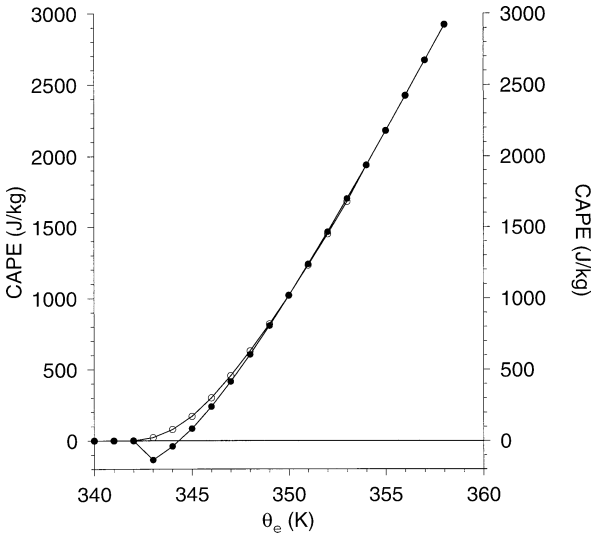

FIG. 10. The dependence of CAPE on surface θ_e. The relative humidity of the air parcel at the surface was fixed at 0.75. The background temperature profile was an average from 15°S to 15°N. The curve with open circles refers to the CAPE as calculated from (3) in the text. The curve with open circles was calculated by an integral from the surface rather than from the LFC, i.e., is a sum of the convective inhibition and the CAPE.

5. Large-scale temperature structure

In Fig. 11, the dashed line represents a pseudoadiabat starting from the surface with a temperature of 299.3 K (the 15°S–15°N annual mean) and a relative humidity of 0.76. This pseudoadiabat closely approximates the observed 15°S–15°N annual tropical temperature climatology below 345 K (~11.3 km), but progressively deviates from the temperature climatology above 345 K. The onset of an increase in thermal stratification above 345 K is also shown in Fig. 12. The SHADOZ dataset was used to generate annual temperature climatologies at three different tropical locations. The dependence of lapse rate on potential temperature is shown for each location. All three locations indicate a lapse rate minimum near 345 K (see also Atticks and Robinson 1983).

As the concentration of water vapor goes to zero, a moist adiabat will approach a dry adiabat. Figure 6 shows that the contribution of water vapor to θ_e is es-

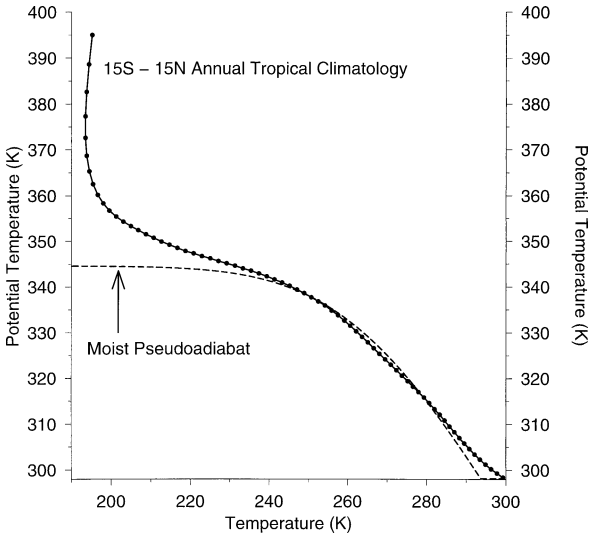

FIG. 11. The curve with solid circles represents a 15°S–15°N annual temperature climatology. The dashed curve is a moist pseudoadiabat, starting from the surface with a temperature of 299.3 K (26.15°C), and a relative humidity of 0.76, corresponding to a θ_e of 344.7 K.

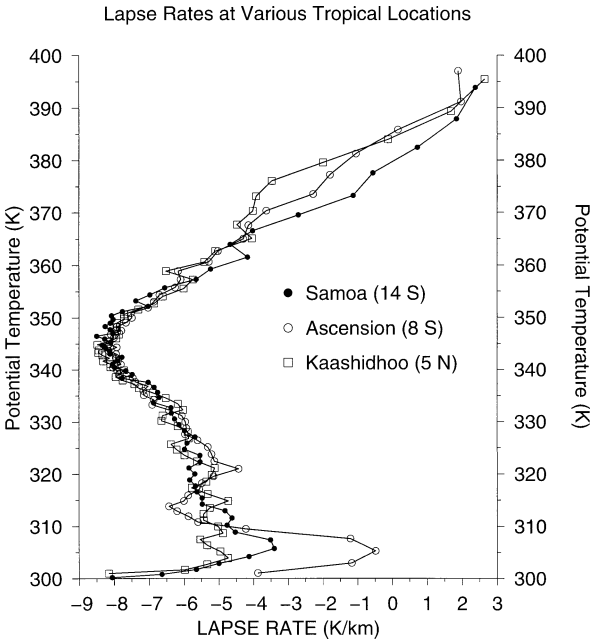

FIG. 12. The dependence of lapse rate (here dT/dz) on potential temperature at three tropical locations. All three locations have a lapse rate minimum near 345 K. The lapse rates were calculated from annual average temperature profiles, except for Kaashidhoo, which is based on measurements from Jan 1999 through Mar 1999, as part of the INDOEX campaign.

sentially zero above 345 K. The persistence of a moist-adiabatic tropical temperature profile above 345 K (now effectively a dry adiabat) would result in an atmosphere that was very near neutral stability. The large increase in convective outflow above 345 K presumably prevents this from happening. That is, that the temperature above 345 K responds in such a way as to maintain a near constant τ_{rem}. A constant τ_{rem} or scaling, could help constrain temperatures in this region because the rate of decrease in the radiative heating rate above 345 K is extremely sensitive to the assumed vertical gradient in temperature and relative humidity.

Figure 13 suggests that the increase in τ_{rem} above 356 K (~15.0 km) is associated with the fact that temperatures above this surface are under increasing stratospheric control. Temperatures in the upper tropical troposphere are colder during Northern Hemisphere winter than summer (Reed and Vlcek 1969; Yulaeva et al. 1994). Figure 13 shows mean $\pm 30°$ temperature profiles for the December–February and June–August seasons. The onset of a difference in the two temperature profiles occurs near 356 K. Based on a 15°S–15°N annual average, the 356-K surface corresponds to 15 km in height, or 134 mb in pressure. Fifteen kilometers also corresponds to the height at which cirrus cloud occurrence becomes correlated with stratospheric wave activity (Boehm and Verlinde 2000), while 125 mb (~358 K) has been identified as the pressure at which temperature fluctuations become significantly correlated with temperature fluctuations at 80 mb (Reid and Gage 1996).

One of the prerequisites for the occurrence of a near constant τ_{rem} is that most of the air parcels convectively injected at a θ surface sink back to the earth's surface. This is usually a good approximation, in part because the Hadley cell is so much larger than the Brewer–Dobson (BD) circulation. But it will break down near the θ at which $M_r(\theta)$ and the BD mass flux become of comparable magnitude. The annually averaged upward

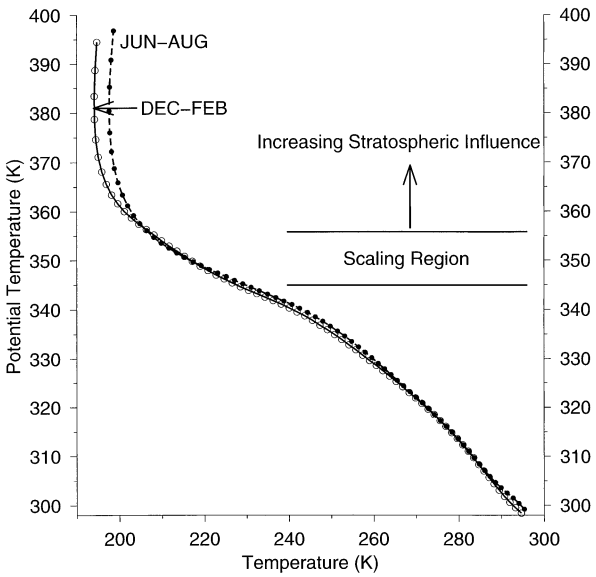

FIG. 13. The solid curve with open circles is a mean 30°S and 30°N Northern Hemisphere winter (Dec–Feb) temperature climatology. The dashed curve with solid circles is a mean 30°S and 30°N Northern Hemisphere summer (Jun–Aug) temperature climatology.

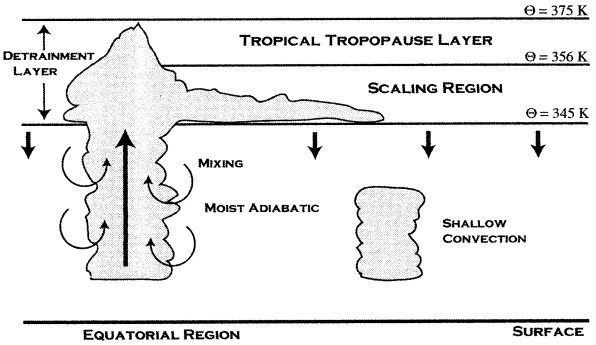

FIG. 14. A schematic overview of the structure of the tropical troposphere. Below 345 K, the temperature profile is maintained near moist adiabatic by shallow convection and by mixing on the sides of deep convective plumes. There is a rapid increase in deep convective outflow in the vicinity of 345 K. Between 345 and 356 K, deep convective outflow decreases with θ at a rate that is roughly proportional to the decrease in the CBL θ_e PDF. This has been labeled the scaling region. Between 356 K (~15.0 km) and 375 K (~16.6 km), the Hadley and Brewer–Dobson mass fluxes are of similar magnitude, and temperatures are under mixed tropospheric and stratospheric control. The entire outflow region from 345 to 375 K is called the detrainment layer.

tropical mass flux at 100 mb has been estimated to be 79.1×10^8 kg s^{-1} (Rosenlof and Holton 1993). Although this mass flux is probably concentrated between $\pm 15°$, it equals 2.73 kg $(m^2\ day)^{-1}$ when averaged over $\pm 30°$. [For comparison, the annually averaged $\pm 30°$ $M_r(\theta)$ at 100 mb is 3.1 kg $(m^2\ day)^{-1}$.] Figure 7 indicates that $M_r(\theta)$ at 345 K is about 300 kg $(m^2\ day)^{-1}$. The Brewer–Dobson mass flux is therefore about 100 times smaller than the Hadley mass flux. Figure 3 indicates that $N(\theta_e)$ has decreased to 0.1 by about 356 K (~15.0 km), so that only about 10% of convective outflow should detrain above this surface. At this point, the Hadley cell is only about 10 times larger than the BD circulation, so that one might expect temperatures above the 356-K surface (~15.0 km) to be under mixed stratospheric and tropospheric control.

Figure 14 gives an overall view of temperature control within the Hadley cell. Below 345 K (~11.3 km), the inner Tropics (roughly 15°S–15°N) are warmed and moistened by shallow convection and by turbulent mixing along the sides of deep convective updrafts. This mixing helps maintain a moist-adiabatic temperature profile, corresponding to the θ_e at which CAPE first becomes positive. The onset of mass flux scaling at 345 K is associated with a large increase in net convective outflow, with the amount of outflow at each potential temperature roughly proportional to the frequency with which that value of θ_e is realized in the boundary layer. Temperatures within the scaling region are controlled by (2), a diagnostic relationship between the radiatively driven convective outflow and the boundary layer θ_e distribution. Shallow convection probably plays an important role in mass flux scaling by diminishing the contrast in θ_e between cloudy and environmental air, making it more likely for subsequent convection to detrain at the LNB.

The layer between 356 K (~15.0 km) and 375 K (~16.6 km) is referred to as the tropical tropopause layer (TTL) (e.g., Highwood and Hoskins 1998; Folkins et al. 1999). It can be considered to be the region in which the BD and Hadley mass fluxes are of comparable magnitude. The top of this layer has been designated to be 375 K, somewhat arbitrarily. From Fig. 3, $N(375\ K) = 0.005$, so that one might expect the convective outflow above 375 K to be approximately half the BD circulation. However the statistical representativeness of the θ_e PDFs is questionable at such high values of θ_e. In addition, convective overshooting could increase the amount of convective outflow at the highest potential temperatures (Danielsen et al. 1993; Sherwood and Dessler 2001).

The notion that the layer between 345 K (~11.3 km) and 375 K (~16.6 km) might be the range of potential temperatures over which most deep convective outflow occurs is roughly consistent with ground-based lidar measurements of mean cloud top and cloud bottom from the 1992–93 TOGA COARE campaign (Sassen et al. 2000). From these measurements, the highest probability of occurrence of cloud base was 12 km, while the highest probability of occurrence of cloud top was 16.85 km. Figure 15 shows a mean profile of potential temperature against height from radiosonde measurements above Misima (off the eastern coast of New Guinea) during the December TOGA COARE period. A mean cloud-base height of 12 km corresponds to $\theta = 348$ K, while a mean cloud-top height of 16.85 km corresponds to $\theta = 368$ K. This roughly corresponds to the range of potential temperatures used to define the detrainment layer (345–375 K). It should be kept in mind, however, that inferring convective outflow from the presence of ice crystals is problematic because mixing will tend to evaporate ice crystals near the cloud base, and because ice associated with the small amounts of convective outflow above the cold point tropopause may evaporate quite quickly as it mixes with warmer ambient air.

Figure 15 also shows mean tropical (15°S–15°N) potential temperature profiles for Northern Hemisphere winter (December–February) and Northern Hemisphere summer (June–August) from the FSL NCDC dataset. The upward displacement of potential temperature surfaces at Misima would be expected to result in cloud tops about 0.5 km higher than other locations in the Tropics that had similar CBL θ_e PDFs. The mean seasonal variation would be expected to result in an additional 0.5-km variation in cloud-top height.

There are obvious analogies between the structure of the tropical troposphere as shown in Fig. 14 and the structure of the CBL. The moist-adiabatic layer below 345 of the tropical troposphere can be considered analogous to the adiabatic subcloud layer below 950 mb of the CBL, while the deep convective detrainment layer from 345 to 375 K can be considered analogous to the

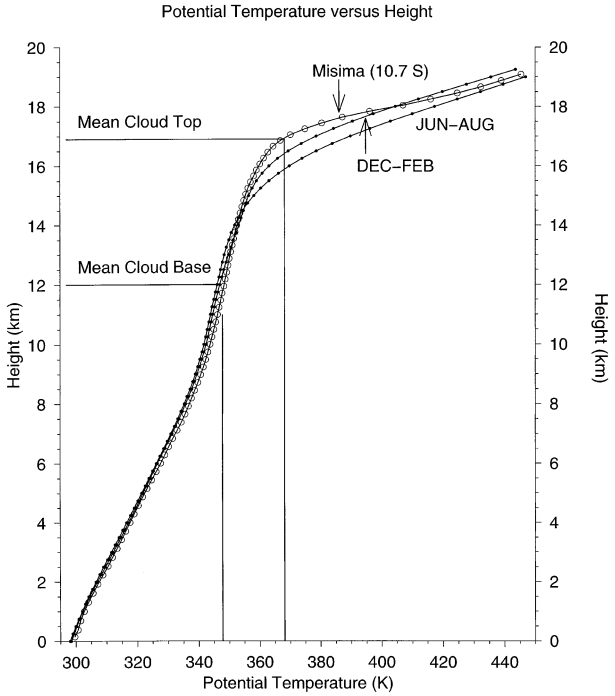

FIG. 15. The curve with open circles is a monthly climatology of potential temperature against height at Misima (off the east coast of New Guinea) obtained from TOGA COARE radiosondes launched during Dec 1992. The average cloud top (16.85 km) and average cloud base (12 km) correspond to the heights with the largest probability of occurrence, as inferred from lidar measurements of deep convective clouds from TOGA COARE (Sassen et al. 2000). The two other profiles correspond to 15°S–15°N seasonal averages from the FSL NCDC archive. Seasonal and regional variations in the relationship between potential temperature and height can be expected to have a significant influence on the mean cloud top at a given tropical location, in addition to variations in the local θ_e PDFs.

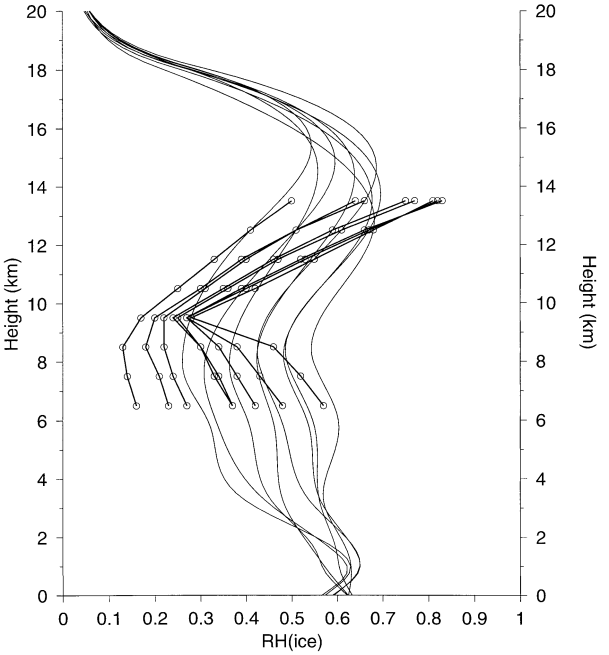

FIG. 16. The thin curves correspond to the variation of RH_{ice} used in the radiative transfer routine to generate $M_r(\theta)$ for various months and latitude ranges. They are constrained by radiosonde observations below 8 km, by MLS measurements at 12.5 km, and by a constant stratospheric water vapor mixing ratio above 18 km. The eight curves correspond to averages from 20°S to the equator, or from the equator to 20°N, for four seasonal time periods. The curves with open circles correspond to MLS observations in the same two latitude bands and seasonal periods (RW01). Near the surface, $RH_{water} = 0.79$.

cloud layer between 950 and 800 mb of the CBL (see also Sherwood and Dessler 2001).

6. Vertical distribution of relative humidity

The decrease in $M_r(\theta)$ above 345 K shown in Fig. 7 is mainly caused by a decrease in the emission of longwave radiation by water vapor. A more rapid decrease in temperature or water vapor above 345 K would give rise to a more rapid decrease in $M_r(\theta)$. Although the existence of scaling is very sensitive to the specification of water vapor between 11 and 17 km, there are unfortunately very few measurements of water vapor in this region. Figure 16 shows MLS measurements of relative humidity over ice at 1-km intervals from 6.5 to 13.5 km (RW01). Each curve corresponds to an average from 20°S to the equator, or from the equator to 20°N, for one of four monthly periods: December–February, March–May, June–August, or September–November. The thinner lines denote the RH_{ice} used as inputs into the radiative transfer model for the same eight latitudinal and monthly averages. As mentioned earlier, the RH_{ice} of the model is constrained by radiosonde measurements below 8 km, by the MLS measurement at 12.5 km, and by a constant stratospheric water vapor mixing ratio above 18 km. (When the radiative transfer model is also constrained by the MLS measurements at 13.5 km, the spline interpolation tends to generate values of RH_{ice} larger than 1 between 13.5 and 18 km.) The MLS measurements indicate a sharp increase in RH_{ice} above 9.5 km. This is also present in the model profiles, but to a lesser degree. This increase may be associated with increased moistening within the detrainment layer by convective outflow. This increase in RH_{ice} partially mitigates the decreases in water vapor associated with the cooling temperatures, and makes $M_r(\theta)$ decrease less rapidly with θ in this region.

7. Mass exchange with midlatitudes

The existence of a proportionality, or scaling, between $dN(\theta_e)/d\theta_e$ and $dM_r(\theta)/d\theta$ between 345 and 356 K requires that the net convective outflow between two θ surfaces be much larger than the exchange of mass of that layer with midlatitudes. This assumption has been examined using winds from the FSL NCDC archive. The net flow of mass out of a given volume element

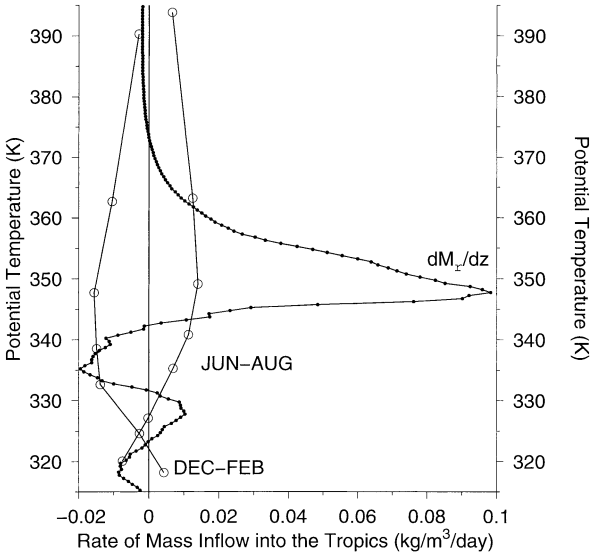

FIG. 17. The curve with solid circles shows the vertical divergence of the 1999 clear sky radiative mass flux dM_r/dz, averaged from 30°S to 30°N. The curves with open circles give the rate of 1999–2000 inflow (positive) or outflow (negative) of mass from the midlatitudes to the Tropics, calculated from (4) in the text.

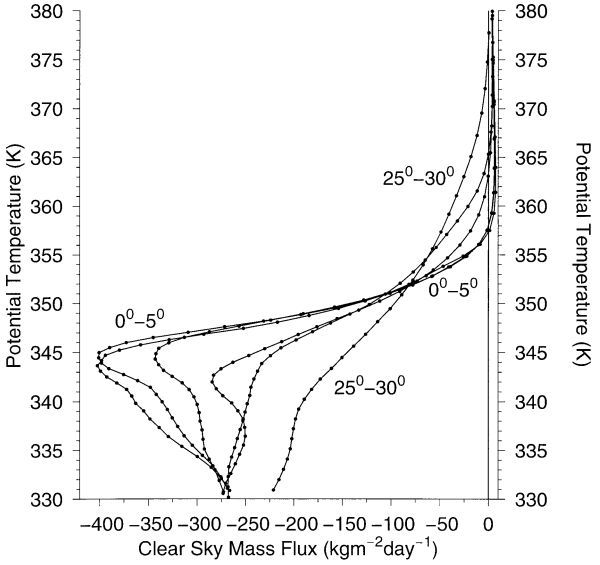

FIG. 18. Each curve represents $M_r(\theta)$ calculated using a different 2000 latitudinal interval temperature average. The largest downward mass fluxes occur for the averages closest to the equator. The latitude ranges are 0°–5°, 5°–10°, 10°–15°, 15°–20°, 20°–25°, and 25°–30°, using in each case an average from both sides of the equator.

within a ±30° interval associated with horizontal transport (HT) is approximately given by

$$\mathrm{HT}(p) = \frac{\overline{\rho v}_{p,30^\circ\mathrm{N}} - \overline{\rho v}_{p,30^\circ\mathrm{S}}}{\frac{1}{3}\pi R_e}, \qquad (4)$$

where ρ is the density at pressure p, v is the meridional velocity, and R_e is the radius of the earth. The mass flux averages $\overline{\rho v}$ were evaluated on the standard pressure levels. For 30°N, we used measurements between 25° and 35°N, while for 30°S we used measurements between 25° and 35°S. Profiles of $HT(p)$ for the December–February, and June–August seasons, using all data from 1999 and 2000, are plotted in Fig. 17. Between 345 and 356 K, the component of the convective outflow balanced by radiative cooling $[dM_r(\theta)/dz]$ is much larger than the outflow associated with midlatitude exchange. Within the TTL however (356–375 K), exchange with midlatitudes can be expected to be comparable with, or larger than convective outflow, at least over seasonal timescales.

Figure 17 indicates that, in the upper tropical troposphere, there is an inward transport of mass from the midlatitudes to the Tropics in the June–August time period, and an outward transport of mass from the Tropics during December–February. This conclusion could however be biased by the fact that the number of stations reporting both wind and temperature measurements in the 25°–35°S interval is so much smaller than the 25°–35°N interval.

8. Stratosphere–troposphere exchange

Stratosphere–troposphere exchange (STE) in the Tropics is poorly understood. In part this is because $M_r(\theta)$ is not a good approximation of the vertical mass flux in the vicinity of the potential temperature at which the radiative mass flux goes to zero, $\theta_{Q_r=0}$. Processes that are not significant at other altitudes can be of first-order importance to the energy budget near $\theta_{Q_r=0}$. In particular, one might expect cloud radiative effects (Danielsen 1993; Ackerman et al. 1988), subvisible cirrus (Rosenfield et al. 1998), or the quasi-horizontal transport of heat between the Tropics and midlatitudes by eddies to perturb the heat budget in this region. The notion that one might treat the Hadley cell as an isolated circulation in which mass exchange with higher latitudes can be ignored also breaks down near $\theta_{Q_r=0}$. It is useful however to discuss clear sky radiative forcings in the vicinity of $\theta_{Q_r=0}$ in order to appreciate what a more complete theory of STE in the Tropics might need to consider.

Figure 18 shows annually averaged clear sky mass fluxes $M_r(\theta)$ in the latitudinal bands of 0°–5°, 5°–10°, 10°–15°, 15°–20°, 20°–25°, and 25°–30°. Mass fluxes defined within the latitudinal bands closer to the equator peak at a larger value, decrease more rapidly with potential temperature, and have a lower $\theta_{Q_r=0}$. The more rapid decrease in $M_r(\theta)$ closer to the equator is associated with a more rapid decrease in temperature, and water vapor concentrations at these latitudes, which gives rise to a steeper gradient in the longwave cooling rate.

The $\theta_{Q_r=0}$ obtained from each of the six mass flux profiles shown in Fig. 18 are plotted versus latitude in

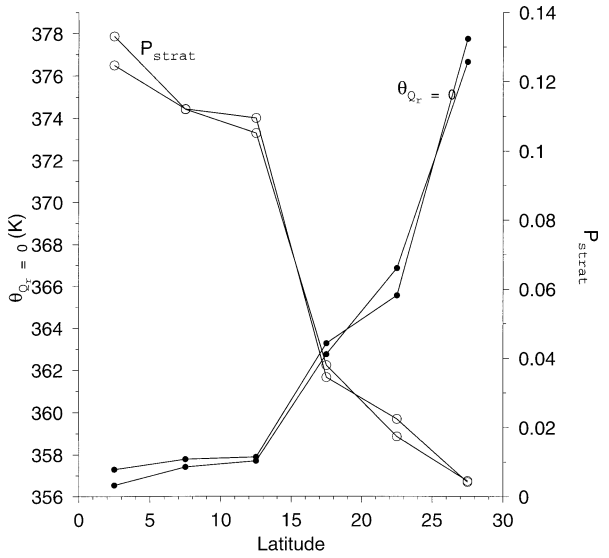

FIG. 19. The curves with solid circles shows the dependence of $(\theta_{Q_r=0})$ on latitude. The $(\theta_{Q_r=0})$ have been inferred from the profiles of $M_r(\theta)$ shown in Fig. 13. They increase sharply at $\pm 15°$. The years 1999 and 2000 have been plotted separately but are very similar. The curves with open circles shows the dependence of P_{strat} on latitude, calculated from (5) in the text. Here P_{strat} is the fraction of near-surface convective air parcels that would ascend into the stratosphere if they detrained near their LNB, and clear sky radiative heating was the only process moving air parcels across potential temperature surfaces.

Fig. 19. Here $\theta_{Q_r=0}$ is nearly constant at about 357 K from 0° to 15°. This is consistent with the notion that by drawing air up into the stratosphere, the BD circulation adiabatically cools the upper tropical troposphere above 356 K, helps drive the heating rates to positive values, perturbs $M_r(\theta)$, and destroys scaling.

There are two reasons why $\theta_{Q_r=0}$ tends to be smaller closer to the equator. One is that θ surfaces within the TTL tend to dome up over convectively active regions and the equator, so that if the $Q_r = 0$ height were independent of latitude, it would tend to be located on a lower θ surface closer to the equator. The other reason is that the $Q_r = 0$ height itself tends to increase from 15.0 km at the equator to about 15.7 km at $\pm 27.5°$.

On clear sky radiative grounds, an air parcel that detrains from a convective cloud below $\theta_{Q_r=0}$ will sink back to the surface, while an air parcel that detrains above $\theta_{Q_r=0}$ will rise into the stratosphere. The fraction of deep convective air parcels that detrain above $\theta_{Q_r=0}$ will be referred to as P_{strat}. It is approximately given by

$$P_{\text{strat}} = \frac{N(\theta_{Q_r=0})}{N(345\ \text{K})}. \tag{5}$$

In Fig. 19 P_{strat} is plotted versus latitude. In the inner Tropics (within 15° of the equator), the fraction of convective air parcels that subsequently radiatively ascend into the stratosphere if they detrained at their LNB is approximately equal to 0.12. However, P_{strat} rapidly decreases for latitudes greater than 15°. On radiative considerations, one would therefore expect ascent from the troposphere to the stratosphere to be largely confined to within 15° of the equator.

If one assumes that convective outflow is evenly dispersed from 30°S to 30°N, then Fig. 19 suggests that about 7% of convective air parcels have sufficient θ_e to detrain above $\theta_{Q_r=0}$. This percentage is significantly larger than the approximately 1% needed to sustain the BD circulation. There are a variety of possible explanations for this overestimate. First, Fig. 5 indicates that the FSL NCDC archive may overestimate $N(\theta_e)$ at large θ_e, at least compared to regions that are associated with active convection. For example, use of the Samoan CDF would give a $P_{\text{strat}} \approx 0.01$. Another possibility is that cirrus clouds increase $\theta_{Q_r=0}$ by reducing the upwelling longwave radiation from the surface (e.g., Dessler et al. 1996). Heating rates near $\theta_{Q_r=0}$ can be expected to be particularly sensitive to cloud effects because solar heating is extremely small. Even a modest reduction in longwave heating would result in an upward shift in $\theta_{Q_r=0}$ of a few degrees, sufficient to significantly reduce P_{strat}. A third possibility is that some of the air that detrains from convective clouds above $\theta_{Q_r=0}$ is transported horizontally to latitudes higher than $\pm 30°$. And finally, mixing with lower θ_e air during ascent would diminish detrainment above $\theta_{Q_r=0}$.

9. Discussion and conclusions

The tropical troposphere is often thought of as a well-mixed layer with a ''lid''—the tropopause—which delineates it from the stratosphere. We have tried to motivate a thermodynamically based statistical picture of the interface between the troposphere and the stratosphere. Below 345 K (~11.3 km), the tropical troposphere can be considered to be well mixed with a mean temperature profile that approximates a pseudoadiabat. At 345 K, the mean temperature profile starts to deviate from a pseudoadiabat. This corresponds to the θ_e at which air parcels in the CBL first have positive CAPE, and is associated with a rapid increase in net convective outflow. Between 345 K (~11.3 km) and 356 K (~15.0 km), net convective outflow appears to diminish in a quasi-exponential manner, roughly proportional to the falloff in the CBL θ_e PDF. We have referred to this behavior as scaling. Within the scaling region, one can expect the CBL θ_e PDF, convective outflow, water vapor concentrations, and the temperature profile to be strongly coupled. The layer between 356 K (~15.0 km) and 375 K (~16.6 km) has been referred to as the tropical tropopause layer (TTL). Within the TTL, the Hadley and BD mass fluxes appear to be of similar magnitude, so that both circulations have some influence on the temperature profile. The term detrainment layer was introduced for the entire range of potential temperatures (345–375 K) over which net convective outflow in the Tropics is likely to occur.

A sharply peaked maximum in convective detrain-

ment in the upper tropical troposphere has been previously inferred from an analysis of arrays of radiosondes (Yanai et al. 1973). It has also been previously argued that while deep convection appears to require a minimum CAPE of 300 J kg^{-1} (corresponding to a threshold θ_e of 346 K), the likelihood of deep convection does not respond to additional increases in CAPE (Sherwood 1999). This is consistent with a near constant τ_{rem} within the scaling region.

The existence of scaling is consistent with a very simple picture of the overturning Hadley cell: that mass exchange with midlatitudes can be neglected compared to convective outflow, the rate of subsidence can be inferred from clear sky radiative heating, the timescale for removal of an air parcel from the boundary layer by deep convection is independent of θ_e once its θ_e exceeds 345 K, and air parcels subject to deep convection detrain near their LNB. It should be kept in mind that these properties refer to the $\pm 30°$ Hadley cell as a whole rather than individual convective events, and that other explanations of scaling are possible. This simple picture of the Hadley cell has been invoked as a heuristic way of explaining the existence of scaling, but it is unclear why scaling occurs, given that many of these conditions appear to be violated by tropical storms. Although scaling may prove useful as a way of explaining the variation of temperature with height in the scaling interval, water vapor mixing ratios in the 345–356-K interval are not yet sufficiently well characterized at this point to believe that it is more than an approximate relationship.

In addition to influencing the temperature structure of the upper tropical troposphere, the distribution of θ_e in the boundary layer also has an influence on the mechanisms whereby stratosphere–troposphere exchange is likely to occur. Of particular interest is the number of air parcels in the boundary layer whose θ_e is larger than the θ at which clear sky radiative heating rates first become positive. If this number is smaller than that needed to sustain the Brewer–Dobson circulation, one would be required to invoke convective overshooting (Danielsen 1993), or other additional heat sources, as mechanisms whereby air parcels are transported into the stratosphere. Although convective overshooting and irreversible mixing undoubtedly occur, we have argued that there appears to be more than enough high θ_e air parcels in the CBL to sustain the Brewer–Dobson circulation simply by detrainment at the LNB followed by subsequent mean upward ascent associated with clear sky radiative heating. This conclusion is however sensitive to cloud radiative effects, the shape of $N(\theta_e)$ at the high θ_e tail, and to the approximations made in using pseudoequivalent potential temperature as an indicator of the LNB of an air parcel. More measurements of θ_e in the tropical regions where deep convection occurs, and on the composition of tropical clouds in the vicinity of 360 K, would be desirable.

Acknowledgments. We are grateful for the use of the Forecast Systems Laboratory National Climatic Data Center Radiosonde Data Archive (http://raob.fsl.noaa.gov/Raob_Software.html). This research was supported by the Natural Sciences and Engineering Research Council of Canada. I. F. thanks Glen Lesins for many discussions, and Steven Sherwood for many suggestions that helped improve the manuscript.

REFERENCES

Ackerman, T. P., K. N. Liou, F. P. J. Valero, and L. Pfister, 1988: Heating rates in tropical anvils. *J. Atmos. Sci.,* **45,** 1606–1623.

Anderson, G. P., S. A. Clough, F. X. Kneizys, J. H. Chetwynd, and E. P. Shettle, 1986: AFGL atmospheric constituent profiles (0–120 km). Air Force Geophysics Laboratory Tech. Rep. AFGL-TR-86-0110, Hanscom AFB.

Atticks, M. G., and G. D. Robinson, 1983: Some features of the tropical tropopause. *Quart. J. Roy. Meteor. Soc.,* **109,** 295–308.

Betts, A. K., and W. Ridgway, 1989: Climatic equilibrium of the atmospheric convective boundary layer over a tropical ocean. *J. Atmos. Sci.,* **46,** 2621–2641.

Boehm, M. T., and J. Verlinde, 2000: Stratospheric influence on upper tropospheric tropical cirrus. *Geophys. Res. Lett.,* **27,** 3209–3212.

Bolton, D., 1980: The computation of equivalent potential temperature. *Mon. Wea. Rev.,* **108,** 1046–1053.

Chimonas, G., and R. Rossi, 1987: The relationship between tropopause potential temperature and the buoyant energy of storm air. *J. Atmos. Sci.,* **44,** 2902–2911.

Danielsen, E., 1993: In situ evidence of rapid, vertical, irreversible transport of lower tropospheric air into the lower tropical stratosphere by convective cloud turrets and by larger-scale upwelling in tropical cyclones. *J. Geophys. Res.,* **98,** 8665–8681.

Dessler, A. E., 1998: A reexamination of the ''stratospheric fountain'' hypothesis. *Geophys. Res. Lett.,* **25,** 4165–4168.

——, K. Minschwaner, E. M. Weinstock, E. J. Hintsa, J. G. Anderson, and J. M. Russell III, 1996: The effects of tropical cirrus clouds on the abundance of lower stratospheric ozone. *J. Atmos. Chem.,* **23,** 209–222.

Folkins, I., M. Loewenstein, J. Podolske, S. Oltmans, and M. Proffitt, 1999: A barrier to vertical mixing at 14 km in the Tropics: Evidence from ozonesondes and aircraft measurements. *J. Geophys. Res.,* **104,** 22 095–22 101.

——, S. J. Oltmans, and A. Thompson, 2000: A relationship between convective outflow and surface equivalent potential temperatures in the Tropics. *Geophys. Res. Lett.,* **27,** 2549–2552.

Fu, Q., and K. N. Liou, 1992: On the correlated *k*-distribution method for radiative transfer in nonhomogeneous atmospheres. *J. Atmos. Sci.,* **49,** 2139–2156.

Gamache, J. F., and R. A. Houze Jr., 1982: Mesoscale air motions associated with a tropical squall line. *Mon. Wea. Rev.,* **110,** 118–135.

Highwood, E. J., and B. J. Hoskins, 1998: The tropical tropopause. *Quart. J. Roy. Meteor. Soc.,* **124,** 1579–1604.

Johnson, R. H., 1982: Vertical motion in near-equatorial winter monsoonal circulations. *J. Meteor. Soc. Japan,* **60,** 682–689.

Logan, J. A., 1999: An analysis of ozonesonde data for the troposphere: Recommendations for testing 3-D models, and development of a gridded climatology for tropospheric ozone. *J. Geophys. Res.,* **104,** 16 115–16 149.

Read, W. G., J. W. Waters, D. L. Wu, E. M. Stone, Z. Shippony, A. C. Smedley, and C. C. Smallcomb, 2001: UARS MLS upper tropospheric humidity measurement: Method and validation. *J. Geophys. Res.,* in press.

Reed, R. J., and C. L. Vlcek, 1969: The annual temperature variation in the lower tropical stratosphere. *J. Atmos. Sci.,* **26,** 163–167.

Reid, G. C., and K. S. Gage, 1981: On the annual variation in the height of the tropical tropopause. *J. Atmos. Sci.,* **38,** 1928–1938.

——, and ——, 1996: The tropical tropopause over the western Pacific: Wave driving, convection, and the annual cycle. *J. Geophys. Res.,* **101,** 21 233–21 241.

Rosenfield, J. E., D. B. Considine, M. R. Schoeberl, and E. V. Browell, 1998: The impact of subvisible cirrus clouds near the tropical tropopause on stratospheric water vapor. *Geophys. Res. Lett.,* **25,** 1883–1886.

Rosenlof, K. H., and J. R. Holton, 1993: Estimates of the stratospheric residual circulation using the downward control principle. *J. Geophys. Res.,* **98,** 10 465–10 479.

Sassen, K., R. P. Benson, and J. D. Spinhirne, 2000: Tropical cirrus cloud properties derived from TOGA/COARE airborne polarization lidar. *Geophys. Res. Lett.,* **27,** 673–677.

Selkirk, H. B., 1993: The tropopause cold trap in the Australian monsoon during STEP/AMEX 1987. *J. Geophys. Res.,* **98,** 8591–8610.

Sherwood, S. C., 1999: Convective precursors and predictability in the tropical western Pacific. *Mon. Wea. Rev.,* **127,** 2877–2991.

——, and A. E. Dessler, 2001: A model for transport across the tropical tropopause. *J. Atmos. Sci.,* **58,** 765–779.

Williams, E., and N. Renno, 1993: An analysis of the conditional instability of the tropical atmosphere. *Mon. Wea. Rev.,* **121,** 21–36.

Yanai, M., S. Esbensen, and J. Chu, 1973: Determination of bulk properties of tropical cloud clusters from large-scale heat and moisture budgets. *J. Atmos. Sci.,* **30,** 611–627.

Yulaeva, E., J. R. Holton, and J. M. Wallace, 1994: On the cause of the annual cycle in the tropical lower stratospheric temperature. *J. Atmos. Sci.,* **51,** 169–174.